The Thesis Committee for Chang Lu
Certifies that this is the approved version of the following thesis:

Elasticity of single-crystal iron-bearing pyrope to 20 GPa and 750 K

APPROVED BY
SUPERVISING COMMITTEE:

Supervisor:

Jung-Fu Lin

Stephen P Grand

John C Lassiter

Elasticity of single-crystal iron-bearing pyrope to 20 GPa and 750 K

by

Chang Lu, B.S.

Thesis

Presented to the Faculty of the Graduate School of

The University of Texas at Austin

in Partial Fulfillment

of the Requirements

for the Degree of

Master of Science in Geological Sciences

The University of Texas at Austin

May 2012

Dedication

To my parents

For their love, support, and encouragement.

Acknowledgements

In the first place, I would like to express my gratitude to my supervisor Jung-Fu Lin for his leadership, support and supervision over past two years. It is him who taught me how to do scientific research. He is always being there to provide me useful suggestions whenever I meet trouble. Without his patience and encouragement, my M.S. journey would not be so exciting.

I thank Stephen P Grand and John C Lassiter who serve as members of my supervising committee. Their advice and helpful comments helped me a lot in my thesis writing. I also have benefited tremendously from their lectures in these two years.

I gratefully acknowledge Zhu Mao, the postdoc fellow in our mineral physics group, I appreciate Zhu's help for my data processing, writing. She always would like to share her experiences in both doing research and making life, which light up my life when I feel confused about my future.

Many thanks go in particular to my fellows Jin Liu, Junjie Wu, Jing Yang and Nikki Seymour. They not only help me with conducting experiments but also make my life at Austin much more interesting.

My special thanks go to beamline scientists Kurill Zhuravlev, Sergey Tkachev, Vitali B. Prakapenka and Przemyslaw Dera at GeoSoilEnviroCARS (Sector 13), Advanced Photon Source (APS), Argonne National Laboratroy. They are always glad to help us solve technique problems at any time.

I also would like to thank Eric Kelly, Jianshi Zhou and Luke Marshall at the University of Texas at Austin for their experimental help. Eric woke up very early in the morning and spent a whole day with me to help me analysis the composition of my

sample, while Jianshi Zhou and Luke Marshall from ME department provided a lot of help in identifying the orientation of my sample.

I am grateful for financial support from Jackson School of Geosciences in past two years. My research is also supported by the US National Science Foundation (EAR-0838221, EAR-1056670), the Carnegie/DOE Alliance Center (CDAC) and Energy Frontier Research in Extreme Environments (EFree) to my supervisor, Jung-Fu Lin.

Finally, I would like to thank all the people in Jackson School of Geosciences, and express my apology that I could not mention personally.

Absract

Elasticity of single-crystal iron-bearing pyrope to 20 GPa and 750 K

Chang Lu, MS Geo. Sci.

The University of Texas at Austin, 2012

Supervisor: Jung-Fu Lin

Elastic properties of the major constituent minerals in the Earth's upper mantle at relevant high pressure-temperature (P-T) conditions are crucial for understanding the composition and seismic velocity structures of the region. In this study, we have measured the single-crystal elasticity of natural Fe-bearing pyrope, $Mg_{2.04}Fe_{0.74}Ca_{0.16}Mn_{0.05}Al_2Si_3O_{12}$, using *in situ* Brillouin spectroscopy and X-ray diffraction at simultaneous high P-T conditions up to 20 GPa and 750 K in an externally-heated diamond anvil cell. The derived aggregate adiabatic bulk and shear modulus (K_{S0}, G_0) at ambient conditions are 168.2 (±1.8) GPa and 92.1 (±1.1) GPa, respectively, consistent with literature results. Using the third-order Eulerian finite-strain equation to fit the high P-T data, the derived pressure derivative of the bulk and shear moduli at constant temperature are $(\partial K_S/\partial P)_T$=4.4 (±0.1) and $(\partial G/\partial P)_T$=1.2 (±0.1), respectively. Applying these pressure derivatives, the temperature derivative of these moduli at

constant pressure are also calculated, yielding $(\partial K_S/\partial T)_P$=-18.5(±1.3) MPa/K and $(\partial G/\partial T)_P$=-5.2(±1.1) MPa/K, respectively. Compared to literature values, our results show that addition of 25% Fe in pyrope increases the pressure derivative of the bulk modulus by 7%, but has a negligible effect on other elastic parameters. Extrapolation of our results shows that Fe-bearing pyrope remains almost elastically isotropic at relevant P-T conditions of the upper mantle, indicating that it may not have a significant contribution to seismic *Vp* and *Vs* anisotropy in the upper mantle. Together with the elasticity of olivine and pyroxene minerals in the upper mantle, we have constructed new velocity profiles for two representative compositional models, pyrolite and piclogite, along Earth's upper mantle geotherm. These velocity models show *Vs* profiles consistent with seismic observations, although *Vp* profiles are slightly lower than in seismic models.

Table of Contents

List of Tables

List of Figures

Chapter 1: Introduction

Iron-bearing pyrope is an abundant mineral in the Earth's upper mantle. According to the pyrolitic compositional model, Earth's upper mantle (e.g. up to approximately 400-km depth) is mainly composed of ~63% olivine, ~22% pyroxene, and ~15% garnet by volume (Ringwood 1975; Ita and Stixrude 1992). With increasing depth, garnet would become more abundant (up to ~40 vol%) because pyroxene is expected to transform into majoritic garnet in the transition zone (Ringwood 1967, 1991; Ita and Stixrude 1992; Fei and Bertka 1999). Garnets are also abundantly present in the mineral assemblage of eclogites formed from high-pressure mafic rocks (Poli 1993). Upper-mantle garnets are mainly composed of pyrope ($Mg_3Al_2Si_3O_{12}$), with ~6-23% iron and ~2-15% calcium substituting for magnesium (Rickwood et al. 1968; Sinogeikin and Bass 2002; Lee 2003). The presence of small amounts of Fe^{2+} and Ca^{2+} in the system have been known to affect a number of physical properties of pyrope, including elasticity (e.g. Verma 1960; Sumino and Nishizawa 1978; Suzuki and Anderson 1983), electrical conductivity (e.g. Romano et al. 2006; Dai and Karato 2009), and thermal conductivity (e.g. Kanamori et al. 1968; Giesting and Hofmeister 2002).

Considering the abundance of garnet in the Earth's upper mantle and transition zone, experimental studies on the elasticity of iron-bearing pyrope with a relevant composition at upper-mantle P-T conditions thus have significant implications for constraining seismic observations and for understanding the chemical composition of the deep Earth (e.g. Bass and Anderson 1986; Duffy and Anderson 1989; Cammarano et al.

2003). There have been a number of previous measurements of the elasticity of pyrope-rich garnet at high pressures and room temperature (e.g. Leitner et al. 1980; O'Neil et al. 1991; Chen et al. 1997; Conrad et al. 1999; Sinogeikin and Bass 2000) or at room pressure and high temperatures (e.g. Sumino and Nishizawa 1978; Suzuki and Anderson, 1983; Sinogeikin and Bass, 2002). Additionally, ultrasonic measurements on the sound velocities of polycrystalline Mg-end member pyrope have been reported up to 9 GPa and 1300 K (Gwanmesia et al. 2006, 2007), yet laboratory measurements on the single-crystal elasticity of iron-bearing pyrope at relevant chemical and P-T conditions of the upper mantle are lacking.

In the upper mantle, seismological studies have revealed the existence of global azimuthal (Hess 1964; Raitt et al. 1969), polarized shear wave (*Vs*) anisotropies (Ando et al. 1980; Montagner and Tanimoto 1990) and their regional variations (e.g. Silver and Chan 1991). Montagner and Kennett (1996) have reported shear wave and compressional wave anisotropies of the upper mantle ($\xi=(V_{SH}/V_{SV})^2$, $\varphi=(V_{PV}/V_{PH})^2$) in several global seismic models, where the subscript *H* is the seismic wave velocity in the horizontal direction and the subscript *V* represents the vertical direction. In the AK 135-F Earth model (Kennett 1991; Kennett et al. 1995), for example, ξ decreases from ~1.06 to 1 with increasing depth from the surface to 400 km depth in the upper mantle, while φ increases from ~0.94 to 1. It has been proposed that the observed seismic anisotropy is a result of the lattice-preferred orientation of major minerals in the upper mantle (Kawasaki and Konno 1984; Mainprice and Nicolas 1989). Understanding and interpreting the observed seismic anisotropy thus requires detailed knowledge of the single-crystal elasticity of the

constituent minerals in the upper mantle.

In this study, we have measured the single-crystal elasticity of iron-bearing pyrope with 25 mol% Fe up to 20 GPa and 750 K using *in situ* Brillouin spectroscopy and X-ray diffraction in an externally-heated diamond anvil cell (EHDAC). We have evaluated high P-T and iron compositional effects on the sound velocities of garnet as well as its V_P and *Vs* anisotropies to aid our current understanding of seismic velocity and mineralogical models of the upper mantle.

Chapter 2: Experimental Details

Natural single crystals of Fe-bearing pyrope, $(Mg_{2.04}Fe_{0.74}Ca_{0.16}Mn_{0.05})Al_2Si_3O_{12}$, from East Africa were analyzed for chemical composition by electron microprobe (JEOL 8200) and lattice parameters by X-ray diffraction. These analyses showed that the samples, with a lattice parameter a = 11.504(2) Å, were chemically homogeneous with ~25 mol% Fe, ~5 mol% Ca, and a small amount (~1.7 mol%) of Mn. The orientation of the sample platelets was determined by single-crystal X-ray diffraction (XRD) at the Texas Materials Institute of the University of Texas at Austin and the GSECARS sector of the Advanced Photon Source (APS), Argonne National Laboratory (ANL). Sample platelets were doubled-side polished down to 15-35 μm thick in (110) crystallographic orientation or in a random orientation close to (-0.21, 0.92, 0.34). The use of the (110) platelets permits determination of the elastic constants (C_{11}, C_{12}, C_{44}) along principle <110> and <111> axes, while the platelet with the off-principle orientation was used for further confirmation of the measured elasticity. A single-crystal platelet was loaded into an EHDAC having a Re gasket as the sample chamber and Pt wires as the external resistive heating element. Ne was loaded in the chamber as the pressure medium for all experiments, whereas Au powder was loaded close to the sample as the pressure calibrant (Fei et al. 2007) and ruby spheres next to the sample were used as a pressure scale at high pressures and room temperature (Mao et al. 1978). A K-type thermocouple was attached to the diamond surface approximately 500 μm away from the diamond culet for temperature measurements.

High P-T Brillouin measurements (Appendix A) were performed at the GSECARS of the APS, ANL up to 20 GPa with temperatures of 300, 500, and 750 K. The temperature was kept below 750K to avoid the oxidation of diamonds from heating. To ensure the P-T stabilities of the experiments, we have collected X-ray diffraction patterns of the Au pressure calibrant right before and after each set of Brillouin measurements. No significant shift of the X-ray diffraction patterns was observed indicating that the cell was stable during the measurements. Single-crystal XRD patterns of pyrope were also collected to determine the lattice parameter and density of the sample at high P-T conditions. High-pressure Brillouin measurements at 300 K were also conducted at the Mineral Physics Laboratory of the University of Texas at Austin. The pressure-volume (P-V) equation of state (EoS) (Birch 1947) of the sample at 300 K was also measured using X-ray patterns at the High-Pressure Collaborative Access Team (HPCAT) sector of the APS, ANL.

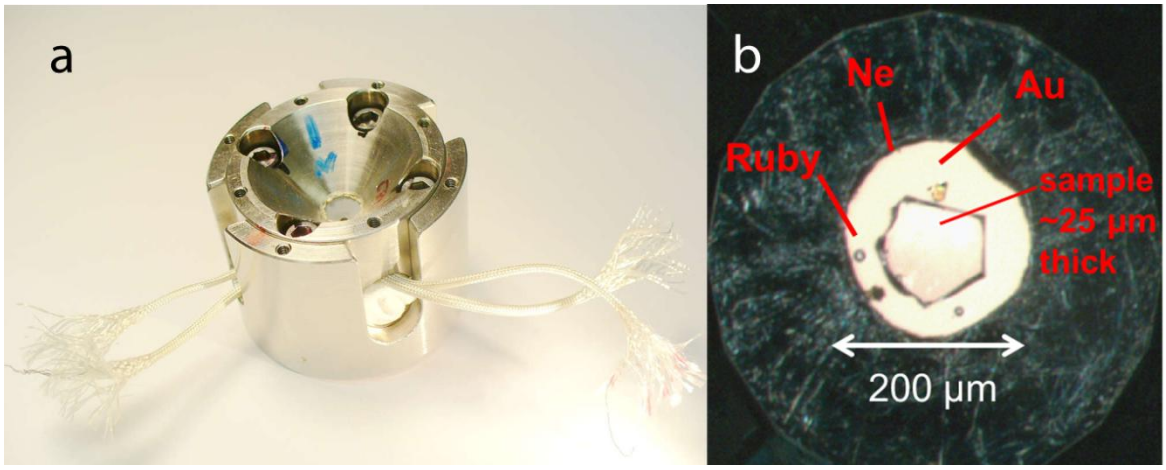

Fig. 1: EHDAC and pyrope sample in EHDAC. (a) externally-heated diamond anvil cell (EHDAC); (b) iron-bearing pyrope sample in EHDAC under 2GPa and 300K.

Chapter 3: Results

High P-T Brillouin and XRD spectra were collected up to 20 GPa and 750 K, in which most of the Brillouin spectra showed strong *Vp* and *Vs* peaks with high signal-to-noise ratios except for some crystallographic directions where *Vp* peaks were weakly observable. Although two polarized *Vs* peaks were expected to exist, only one *Vs* peak was observed in our study, likely a result of two overlapping *Vs* peaks due to small anisotropy (Fig. 2). The variation in *Vp* and *Vs* as a function of the azimuthal angle is not observable outside experimental uncertainties (Fig. 2). Both *Vp* and *Vs* peaks of the Ne medium were also observed at pressures below ~8 GPa, but they were not as visible when pressures were increased. Analyses of the results from the pre-oriented (110) platelets and from off-principle orientation platelets show consistent results for *Vp* and *Vs* within experimental uncertainties.

Single-crystal elastic constants (C_{ij}) of the sample are obtained by fitting the measured acoustic *Vp* and *Vs* velocities to Christoffel's equation using non-linear least squares methods (Every 1980):

$$\left|C_{ijkl}n_j n_l - \rho V^2 \delta_{ik}\right| = 0 \qquad (1)$$

where C_{ijkl} are the elastic constants in full suffix notation which can be simplified using reduced Voigt notation C_{ij}, n_i is the direction cosines of the phonon propagation direction and is described by three Eulerian angles (θ, χ, φ), ρ is the density determined by single-crystal XRD, V is the measured acoustic velocity, and δ_{ik} is the Kronecker delta. As shown in previous studies (e.g. Sinogeikin and Bass 2000), the elastic constants of pyrope can be obtained by averaging the measured acoustic velocities over several non-

symmetric directions, because pyrope is nearly elastically isotropic up to 20 GPa at 300 K (Fig. 2). We note that the elastic constants of Fe-bearing pyrope obtained from the least-squares fitting to the Christoffel's equation are indistinguishable within experimental uncertainties to those derived from averaging the measured velocity assuming isotropic elastic constants (Table 1).

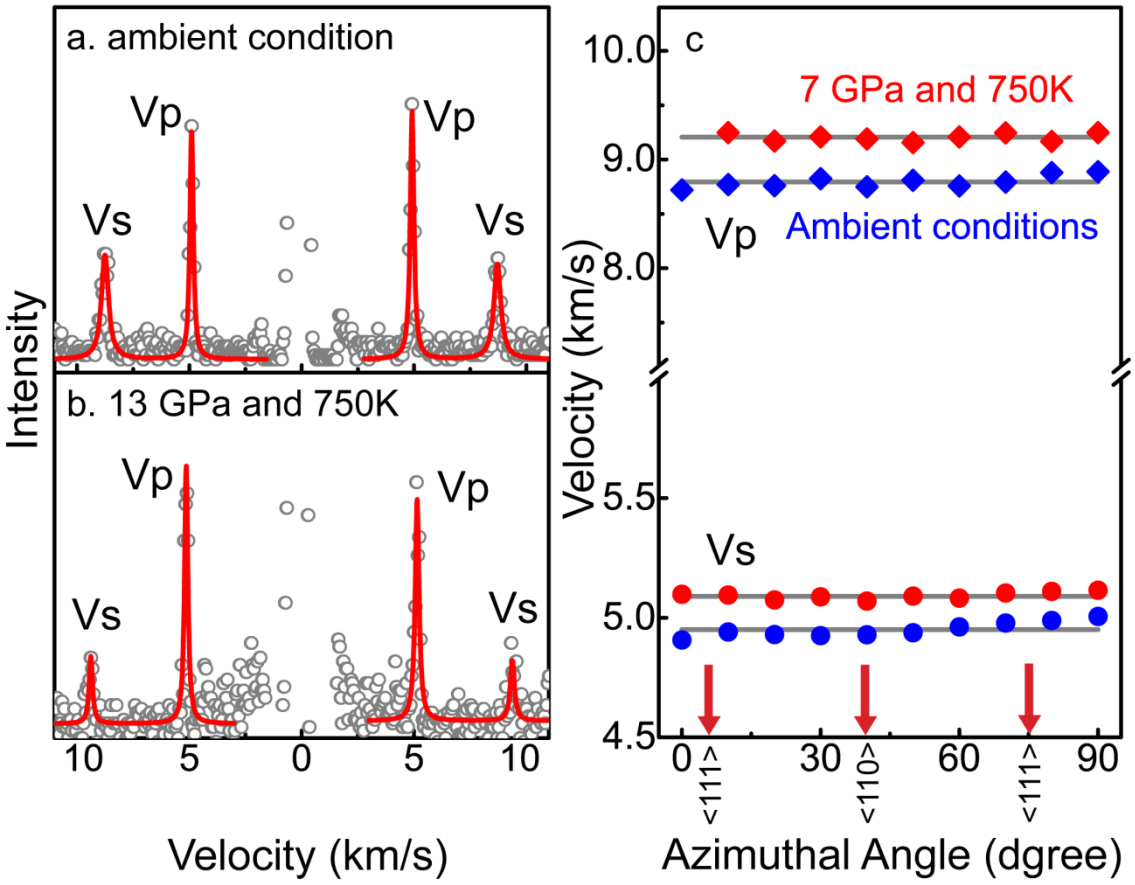

Fig. 2: Representative results from Brillouin scattering measurements. (a) representative Brillouin spectra at ambient condition; (b) representative Brillouin spectra at 13GPa and 750K; (c) *Vp* and *Vs* velocities of the Fe-bearing pyrope as a function of the azimuthal angle in (110) crystallographic orientation platelets. Blue symbols: ambient conditions; red symbols: 7 GPa and 750 K; solid lines: modeled results. Error bars are smaller than the symbols and are not shown. Directions <111>, and <110> are marked.

Table 1: Single-crystal elastic moduli of the Fe-bearing pyrope.

	1 bar, 300K		20 GPa, 750K	
	Fitted[a] C_{ij}	Averaged[b] C_{ij}	Fitted[a] C_{ij}	Averaged[b] C_{ij}
C_{11} (GPa)	290.8(18)	290.9(33)	393.3(24)	395.1(40)
C_{12} (GPa)	107.4(20)	106.8(11)	170.9(24)	168.9(14)
C_{44} (GPa)	92.5(6)	92.1(11)	112.1(10)	113.1(13)
K_s (GPa)	168.5(19)	168.2(18)	245.0(20)	244.3(23)
G (GPa)	91.9(1)	92.1(11)	111.5(3)	113.1(13)

*The comparison indicated that calculated C_{ij} from two methods are indistinguishable within experimental uncertainties.
[a]Fitted C_{ij}: C_{ij} obtained from fitting the measured velocity to the Christoffels' equation.
[b]Averaged C_{ij}: C_{ij} obtained from averaging the measured velocity assuming elastic isotropy of Fe-bearing pyrope.

Using the derived elastic constants of the sample, we have calculated the aggregate adiabatic bulk and shear moduli (K_S and G) using the Voigt-Ruess-Hill averages (Hill 1952). The derived K_{S0} and G_0 at ambient conditions are 168.2 (±1.8) GPa and 92.1 (±1.1) GPa, respectively. The pressure derivatives of the elastic moduli at 300 K were obtained by fitting the moduli at high pressure using the third-order Eulerian finite-strain equation (Birch 1978):

$$K_S = K_{S0}(1+2f)^{\frac{5}{2}}\{1+[3(\frac{\partial K_S}{\partial P})_T - 5]f\} \quad (2)$$

$$G = (1+2f)^{\frac{5}{2}}\{G_0 + [3(\frac{\partial G}{\partial P})_T K_{S0} - 5G_0]f\} \quad (3)$$

$$f = \left(\frac{1}{2}\right)[(\frac{Vol_0}{Vol})^{\frac{2}{3}} - 1] \quad (4)$$

Where $(\partial K_S/\partial P)_T$ and $(\partial G/\partial P)_T$ are the pressure derivatives of the bulk and shear moduli, respectively, at constant temperature, f is the normalized strain, Vol is the unit cell

volume at a given pressure, and Vol_0 is the volume at ambient conditions. Thermal EoS parameters from the literature (Sinogeikin and Bass 2000) were used for calculating the density values for the initial finite-strain fitting. Once $(\partial K_S/\partial P)_T$ was obtained from the modeling, the K_S and $(\partial K_S/\partial P)_T$ were converted to isothermal K_T and $(\partial K_T/\partial P)_T$ using the following thermodynamic relations:

$$K_{T0} = K_{S0}/(1 + \alpha\gamma T) \quad (5)$$

$$(\frac{\partial K_T}{\partial P})_T \approx (1 + \alpha\gamma T)^{-1}[(\frac{\partial K_S}{\partial P})_T - \gamma T/K_{T0}(\frac{\partial K_T}{\partial T})_P] \quad (6)$$

where $(\partial K_T/\partial T)_P$ is the temperature derivative of K_T at constant pressure, α is the volume thermal expansion coefficient (Fei 1995), and γ is the Grüneisen parameter (Gillet et al. 1992). The P-V curve at 300 K from single-crystal X-ray diffraction study was also fitted to the third-order Birch-Murnaghan EoS (Birch 1947) using a fixed $(\partial K_T/\partial P)_T$ from equation (6):

$$P = 3K_{T0}(1 + 2f)^{\frac{5}{2}}\{1 + (\frac{3}{2})[(\frac{\partial K_T}{\partial P})_T - 4]f\} \quad (7)$$

Differences in K_T using equation (5) and equation (7) were further used to improve the trial set of density values. These aforementioned procedures were repeated until both K_T and $(\partial K_T/\partial P)_T$ were self-consistent with satisfactory density values. With the thermal EoS values determined, the pressure derivatives of the three elastic constants and the bulk and shear moduli were derived to be: $(\partial C_{11}/\partial P)_T$=6.0 (±0.1), $(\partial C_{12}/\partial P)_T$=3.6 (±0.1), $(\partial C_{44}/\partial P)_T$=1.2 (±0.1), $(\partial K_S/\partial P)_T$=4.4 (±0.1), and $(\partial G/\partial P)_T$=1.2 (±0.1). Considering the well-known tradeoff between K_{T0} and $(\partial K_T/\partial P)_T$ in third order Birch-Murnaghan EoS fitting, the procedures above are needed to ensure the robustness of our fitting result.

To evaluate the temperature effect under high pressure, a linear equation was applied to obtain the temperature derivatives of the elastic moduli at high pressures due to limited data at high temperature (Gwanmesia et al. 2006, 2007; Irifune et al. 2008):

$$M = M_0 + (P - P_0)(\frac{\partial M}{\partial P})_T + (T - T_0)(\frac{\partial M}{\partial T})_P \quad (8)$$

where M is either the C_{ij} or the elastic moduli (K_S and G), and P_0 and T_0 are ambient pressure and temperature, respectively. The temperature derivatives of the elastic constants and moduli are: $(\partial C_{11}/\partial T)_P$ =-21.0 (±4.0) MPa/K, $(\partial C_{12}/\partial T)_P$=-15.7 (±0.5) MPa/K, $(\partial C_{44}/\partial T)_P$=-3.0 (±1.4) MPa/K, $(\partial K_S/\partial T)_P$=-17.6 (±2.0) MPa/K and $(\partial G/\partial T)_P$=-3.0 (±1.4) MPa/K (Fig. 3 and 4; Table 2 and 3). We note that the second-order derivatives of the elastic moduli such as $\partial^2 K_S/(\partial P \partial T)$ and $\partial^2 G/(\partial P \partial T)$ of pyrope are expected to be negligible (in the order of 10^{-4} K^{-1}) (Gwanmesia et al. 2007). The temperature derivatives of the elastic moduli were also evaluated with fixed K_{S0} and $(\partial K_S/\partial P)_T$ values from room temperature study in the linear fitting procedure (equation 8), because the M_0 and $(\partial M/\partial P)_T$ values are better constrained at room temperature with more experimental data points. These combined procedures are called the revised linear fitting method in our discussion below for convenience (Table 2 and 3).

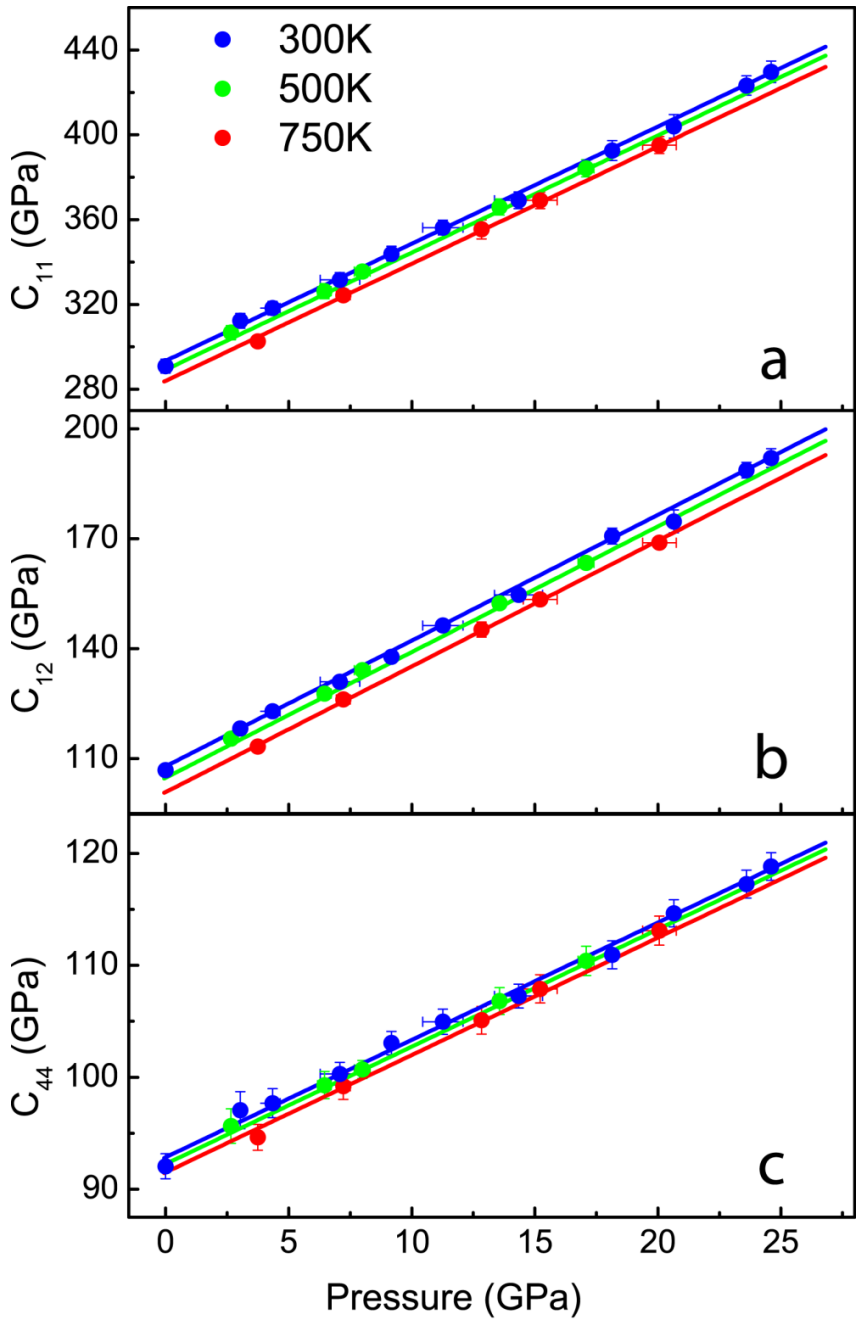

Fig. 3: Single-crystal elastic constants of the Fe-bearing pyrope at high P-T. Blue, green and red circles: experimental values at 300 K, 500 K and 750 K, respectively; blue, green and red solid lines: modeled results at 300 K, 500 K and 750 K, respectively.

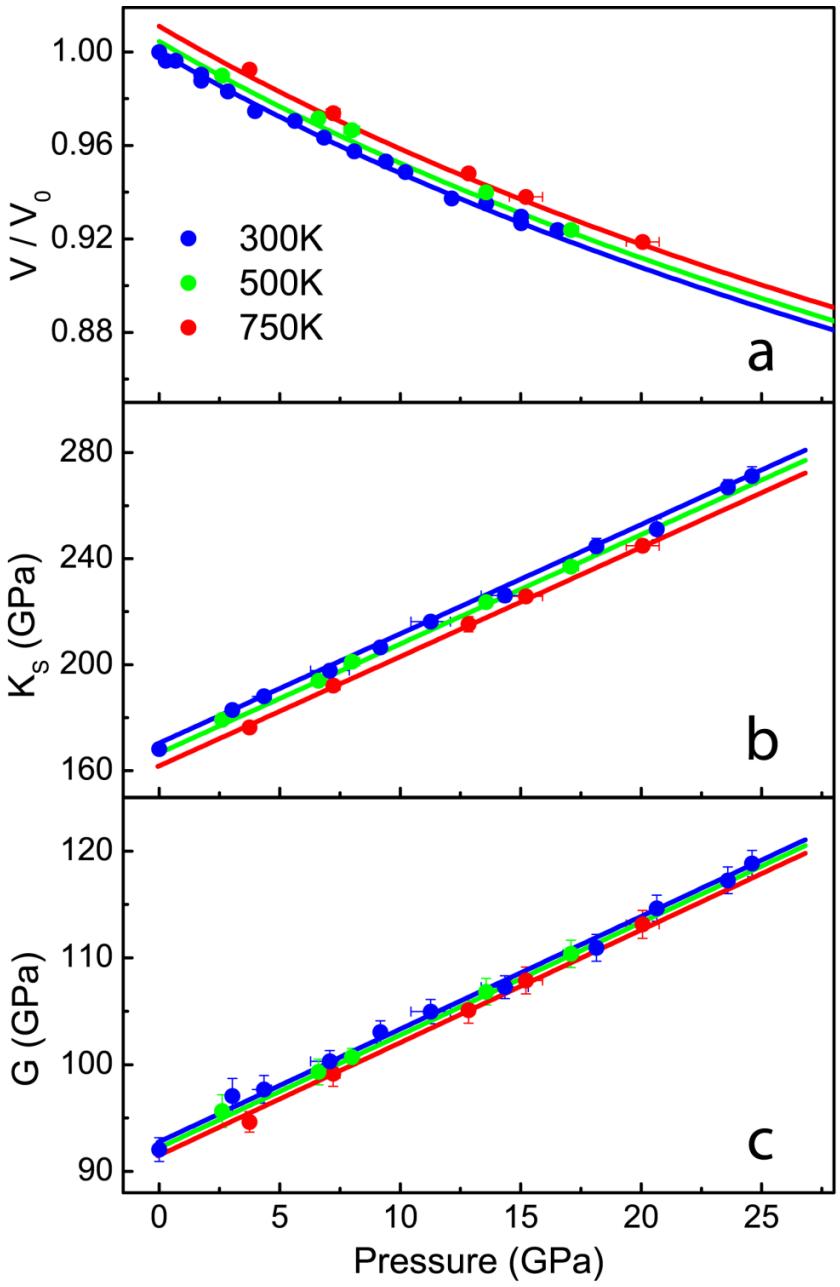

Fig. 4: Equation of state and aggregated bulk and shear moduli of the Fe-bearing pyrope. (a) equation of state of Fe-bearing pyrope; (b) adiabatic bulk modulus, K_S; (c) shear modulus, G. Blue, green and red circles: experimental data at 300 K, 500 K and 750 K, respectively. A third-order Birch-Murnaghan equation of state was applied to fit the data at 300 K (blue), while the high P-T results (500 K and 750 K) were analyzed using the linear fitting (green and red lines).

Table 2: Bulk / shear moduli and their pressure derivatives of the pyrope-rich garnet.

Study	max P (GPa)	Composition	K_S (GPa)	$(\partial K_S/\partial P)_T$	G (GPa)	$(\partial G/\partial P)_T$
Brillouin Scattering						
This study (Revised linear)	24.6	Py68Alm25Gr5Sp1	168.2(18)	4.4(1)	92.1(11)	1.2(1)
This study (linear)	24.6	Py68Alm25Gr5Sp1	169.9(7)	4.1(1)	92.9.1(6)	1.0(1)
Sinogeikin (2000)	20	Py100	171.2(20)	4.1(3)	93.7(20)	1.3(2)
Conrad (1999)	8.75	Py100	172.7	3.22	92	1.4
Leitner (1980)	0	Py100	177(1)		89(1)	
O'Neil (1991)	0	Py100	172.8(3)		92.0(2)	
O'Neil (1991)	0	Py90Alm8Gr3	172.4(7)		93.2(5)	
Jiang (2004)	11	Py20Alm72Gr3Sp3And2	174.9(16)	4.7(3)	95.6(5)	1.4(1)
Ultrasonic Interferometry						
Chen (1999)	10	Py100	171(2)	5.3(4)	92(1)	1.6(2)
Gwanmesia (2006)	8.7	Py100	175(2)	3.9(3)	91(1)	1.7(2)
Gwanmesia (2007)	0.3	Py100	166		92.2(10)	
Wang (2001)	3	Py94Alm6	170.1	4.9	90.2(21)	
Bonczar (1977)	1	Py61Alm36Gr2	168.2(4)	4.7(2)		
Webb (1989)	3	Py61Alm36Gr2	173.6(4)	4.93(6)		
Chai (1997)	20	Py52Alm32Gr15Sp1	170.8(14)	4.09	94.7(6)	1.76
Chen (1997)	0	Py27Alm73	175		99	
Soga (1967)	0.3	Py21Alm76Gr3	177	5.43	94.3(14)	
Verma (1960)	0	Py14Alm81Ca4Sp1	176.5		95.1	
Wang (2001)	3	Alm100	175.1	6.2	92.1(16)	

*Summary of bulk and shear moduli and their pressure derivatives by Brillouin Scattering and Ultrasonic Interferometry methods on pyrope-rich garnet.
**Py: pyrope, $Mg_3Al_2Si_3O_{12}$; Alm: almandine, $Fe_3Al_2Si_3O_{12}$; Gr: grossular, $Ca_3Al_2Si_3O_{12}$; Sp: spessartine, $Mn_3Al_2Si_3O_{12}$.

Table 3: Bulk / shear moduli and their temperature derivatives of the pyrope-rich garnet.

Study	Composition	K_S (GPa)	$(\partial K_S/\partial T)_P$ (MPa/K)	K_T (GPa)	$(\partial K_T/\partial T)_P$ (MPa/K)	G (GPa)	$(\partial G/\partial T)_P$ (MPa/K)
Brillouin Scattering							
This study (Revised linear)	Py68Alm25Gr5Sp1	168.2(18)	-18.5(13)	167.0(18)	-25.4	92.1(11)	-5.1(11)
This study (linear)	Py68Alm25Gr5Sp1	169.9(15)	-17.6(19)	169.1(15)	-24.6	92.8(6)	-3.0(14)
Sinogeikin (2002)	Py100	171(2)	-14(2)	169.4(2)	-19.4(30)	94(2)	-9.2(10)
Ultrasonic Interferometry							
Gwanmesia (2006)	Py100	175(2)	-18(2)	172(2)	-26(4)	91(1)	-10(1)
Gwanmesia (2007)	Py100	166(0.2)	-19.3(4)	164.3	-26	92.1(1)	-10.4(2)
Suzuki (1983)	Py73Alm16And4Uv6	171.2(8)	-19.4	169.4	-25.6	92.6(3)	-10.2
Sumino (1978)	Py73Alm16And4Uv6	171.2(16)	-22.5(12)			92.7(1)	-8.7(3)
Bonczar (1977)	Py62Alm36	168.2(4)	-18.8(6)				
Sumino (1978)	Py50Alm46Gr2And1	173.6(16)	-22.7(25)			95.3(1)	-10.7(3)
Sumino (1978)	Py39Alm54Gr5And1	173.5(12)	-22.7(23)			95.5(1)	-10.9(3)
Soga (1967)	Py21Alm76Gr3	177	-20.1			94.3	-10.6

*Summary of bulk and shear moduli and their pressure derivatives by Brillouin Scattering and Ultrasonic Interferometry methods on pyrope-rich garnet.
**Py: pyrope, $Mg_3Al_2Si_3O_{12}$; Alm: almandine, $Fe_3Al_2Si_3O_{12}$; Gr: grossular, $Ca_3Al_2Si_3O_{12}$; Sp: spessartine, $Mn_3Al_2Si_3O_{12}$.

Chapter 4: Discussion

THE EFFECT OF IRON ON THE ELASTICITY OF PYROPE AT HIGH P-T

In order to understand the effect of Fe on the elasticity of the pyrope-almandine joint, we have compared our results to literature values obtained from Brillouin scattering and ultrasonic interferometer measurements (Fig. 5, 6; Table 2) (Verma 1960; Soga, 1967; Bonczar and Graham 1977; Leitner et al. 1980; Webb 1989; O'Neil et al. 1991; Chai et al. 1997a; Chen et al. 1997, 1999; Conrad et al. 1999; Sinogeikin and Bass 2000; Wang and Ji 2001; Jiang et al. 2004; Gwanmesia et al. 2006, 2007). Here the potential effect of Ca and Mn on the elasticity of pyrope is not considered because of their limited amounts in the studied samples. At ambient conditions, comparative analyses of these results show that addition of Fe does not show a visible effect on the K_S, G and $(\partial G/\partial P)_T$ of pyrope within experimental uncertainties, although increasing the Fe content in pyrope appears to have a weak positive effect on the $(\partial K_S/\partial P)_T$ in results obtained from the same Brillouin technique (Fig. 5). Specifically, our derived $(\partial K_S/\partial P)_T$ for pyrope with 25% Fe is ~7% greater than that of pyrope (Sinogeikin and Bass 2000), but ~6% lower than that with 72% Fe (Jiang et al. 2004). We also notice that the results from different studies on the same sample using similar methods may also vary a lot (K_{S0} of pure pyrope by Brillouin scattering, for example), which may due to the differences in experimental details, such as the sample quality, calibration of system, etc.

Because there is a well-known tradeoff between the derived elastic modulus and its pressure derivative values in EoS fittings, we have plotted the *Ks* and *G* of three representative compositions in pyrope-almandine system at high pressures using

Brillouin scattering results (Fig. 6). Comparison of pure pyrope and our results shows that adding 25 mol% Fe to pyrope does not affect the bulk modulus but may slightly reduce the shear modulus at high pressures, while previous study on pyrope with 72 mol% Fe by Jiang et al. (2004) shows that adding Fe will increase both bulk and shear modulus.

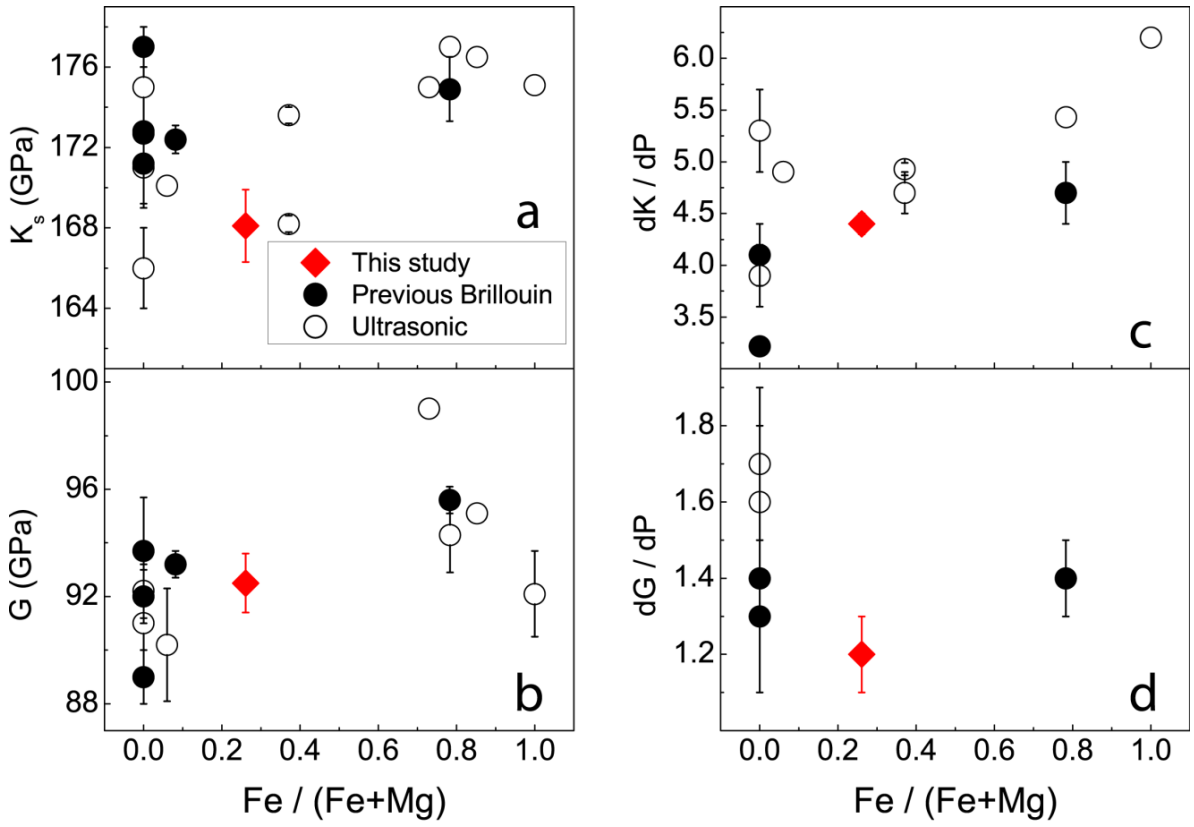

Fig. 5: Experimentally measured bulk and shear moduli in the pyrope-almandine system. (a) bulk modulus, K_{S0}; (b) shear modulus, G_0; (c) pressure derivative of the bulk modulus at 300 K, $(\partial K_S/\partial P)_T$; (d) pressure derivative of the shear modulus at 300 K, $(\partial G/\partial P)_T$. Red circles: this study; black filled circles: previous studies by Brillouin scattering (Leitner et al. 1980; O'Neil et al. 1991; Conrad et al. 1999; Sinogeikin and Bass 2000, Jiang et al. 2004); open circles: previous studies by ultrasonic method (Verma 1960; Soga 1967; Bonczar and Graham 1977; Webb 1989; Chen et al. 1997, 1999; Wang and Ji 2001; Gwanmesia et al. 2006,2007).

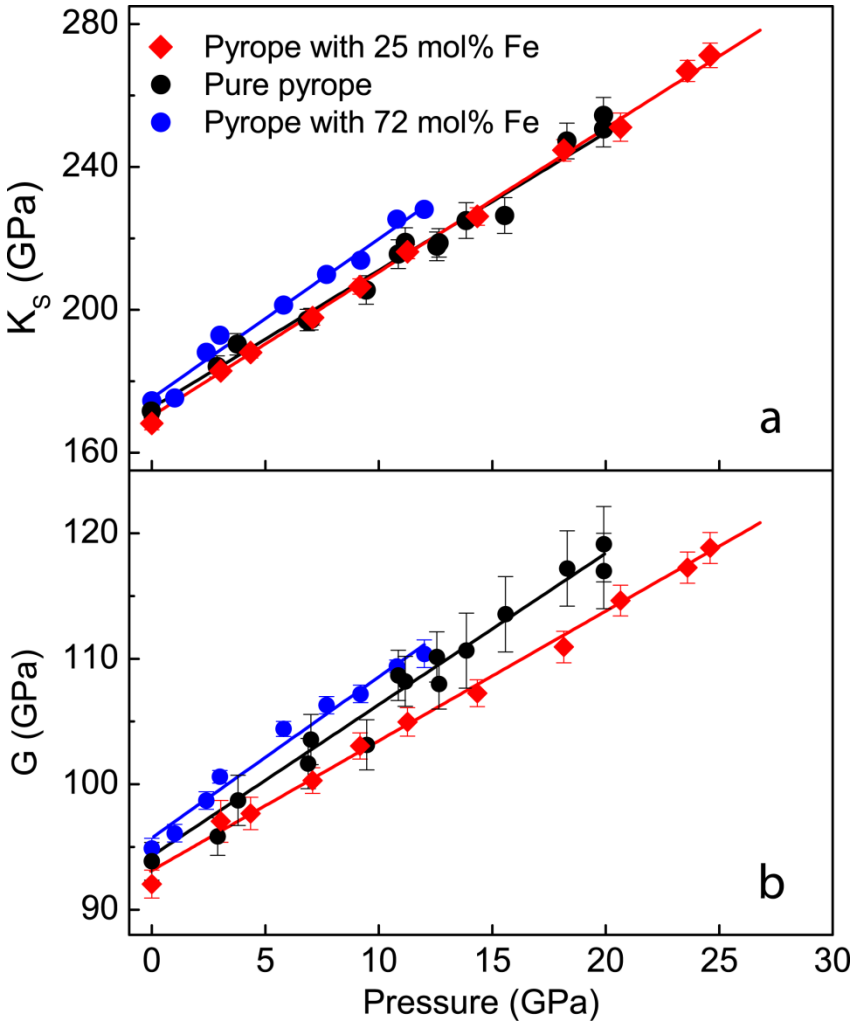

Fig. 6: Comparison of the adiabatic bulk (K_S) and shear moduli (G) in garnet system at high pressure from Brillouin scattering studies. Black circles: pyrope with 25 mol% Fe, to 25 GPa, this study; red circles: Pure pyrope, to 20 GPa (Sinogeikin and Bass 2000); green circles: Pyrope with 72 mol% Fe, to 11 GPa (Jiang et al. 2004).

Jacobsen et al. (2002) have reported that the Fe effect on elasticity in some single-crystal minerals may not be a simple linear effect. In their study, adding Fe to MgO can increase its bulk moduli at first then start to reduce it gradually. Thus this may explain the conflict between our study and the results from Jiang et al. (2004). Due to the lack of systematic

studies on the pyrope-almandine samples using similar experimental techniques and conditions, the Fe effect on elasticity in pyrope is still unclear.

We have also compared the temperature derivatives of the bulk and shear moduli in Fe-bearing pyrope to the literature results (Table 3) (Soga 1967; Bonczar and Graham 1977; Sumino and Nishizawa 1978; Suzuki and Anderson 1983; Sinogeikin and Bass 2002; Gwanmesia et al. 2006, 2007). Our derived $(\partial K_S/\partial T)_P$ for Fe-bearing pyrope is in good agreement with that determined by the ultrasonic method for pure-pyrope within experimental uncertainties (e.g. Singogeikin and Bass 2002; Gwanmesia et at. 2006), but is slightly greater than that obtained from previous Brillouin results at ambient pressure (Sinogeikin and Bass 2002). Due to the relatively small temperature effects involved, it remains unclear if the difference in $(\partial K_S/\partial T)_P$ is caused either by the incorporation of Fe alone or by the uncertainties in different techniques. These all require further examination through high-temperature, high-precision experiments on the pyrope-almandine system. We also note that the effect of temperature on the shear modulus $(\partial G/\partial T)_P$ obtained in this study is much smaller than that of previous works (e.g. Singogeikin and Bass 2002; Gwanmesia et at. 2006). Here $(\partial G/\partial T)_P$ was obtained either from the linear fitting or the "revised linear fitting" method. The difference in $(\partial G/\partial T)_P$ between this study and previous work may be partly caused by the tradeoff between G_0, $(\partial G/\partial P)_T$ and $(\partial G/\partial T)_P$ in deriving $(\partial G/\partial T)_P$ from the high P-T measurements. For example, a variation in G_0 by 2% or in $(\partial G/\partial P)_T$ by 15% can result in a 100-200% change in $(\partial G/\partial T)_P$, even though these variations in G_0 or $(\partial G/\partial P)_T$ are still within the experimental uncertainties of the current study, indicating that the precision in these derived parameters are strongly

correlated in both linear or revised linear fitting methods. To better constrain the temperature effect under high pressure conditions, more data points at higher temperatures and more precisely determined thermal equation of states are needed. In order to fulfill this requirement, the improvement in EHDAC technology is desired.

IMPLICATION FOR THE EARTH UPPER MANTLE

With our updated single-crystal elasticity data of iron-bearing pyrope, we are able to evaluate the seismic anisotropy in the upper mantle. Here we have calculated elastic *Vp* and *Vs* anisotropies of the major upper-mantle minerals, including Fe-bearing garnet (this study), olivine (Zha et al. 1998; Liu and Li 2006), orthopyroxene (Frisillo and Barsch 1972; Duffy and Anderson 1989; Chai et al. 1997), and clinopyroxene (Frisillo and Barsch 1972; Levien et al. 1979; Matsui and Busing 1984; Collins and Brown 1998) at relevant P-T conditions ranging from 200 km to 400 km depth (Stacey 1992). The region above 200 km was not considered in the calculations here because of the complexity in mineral assemblage, chemical heterogeneity and large seismic heterogenity.

The maximum anisotropy (*A*) of each given mineral is calculated following the method in Mainprice et al. (2000):

$$A = 2 \times \frac{V_{max} - V_{min}}{V_{max} + V_{min}} \times 100\% \quad (9)$$

where V_{max} and V_{min} represent the maximum and minimum *Vp* or *Vs* velocity of the mineral, respectively, calculated from its single-crystal elasticity. These values were

further evaluated along an upper mantle geotherm (Stacey 1992) by extrapolating the experimentally measured elastic constants (C_{ij}) and their P-T derivatives to relevant P-T conditions using the third-order Eulerian finite-strain equation (Birch 1978):

$$C_{ijkl}(f) = (1+2f)^{\frac{7}{2}}({C_{ijkl}}^{0} + b_1 f) - P\Delta_{ijkl} \quad (10)$$

$$b_1 = 3K_{S0}\left({C'_{ijkl}}^{0} + \Delta_{ijkl}\right) - 7{C_{ijkl}}^{0} \quad (11)$$

$$\Delta_{ijkl} = -\delta_{ij}\delta_{kl} - \delta_{ik}\delta_{jl} - \delta_{il}\delta_{jk} \quad (12)$$

Our calculations show that both the shear and compressional anisotropies of the Fe-bearing pyrope are extremely small (within 1% for both compression and shear wave). In contrast to the very small anisotropies in garnet, olivine and pyroxene exhibit significantly larger anisotropy in the range of 13% to 32%. Olivine exhibits *A_Vp* = ~21~23% and *A_Vs* = ~14-16%, while pyroxene displays ~13-22% for *A_Vp* and ~17-32% for *A_Vs* (Fig. 7). Due to the extremely small anisotropy of our Fe-bearing pyrope, garnet does not contribute significantly to the seismic anisotropy in the upper mantle region. This confirms previous reports that the seismic anisotropy in the upper mantle is mainly caused by the flow alignment of olivine and pyroxene (Nicolas and Christensen 1987).

To better understand seismic profiles and mineralogical models of the upper mantle, we have also modeled the *Vp* and *Vs* profiles of upper mantle mineral assemblages using updated elastic properties of Fe-bearing pyrope for the Earth's upper mantle region between 200-400 km depth along a normal continental geotherm (Stacey 1992) by extrapolating the elastic moduli (K_S and G) and density value to the P-T

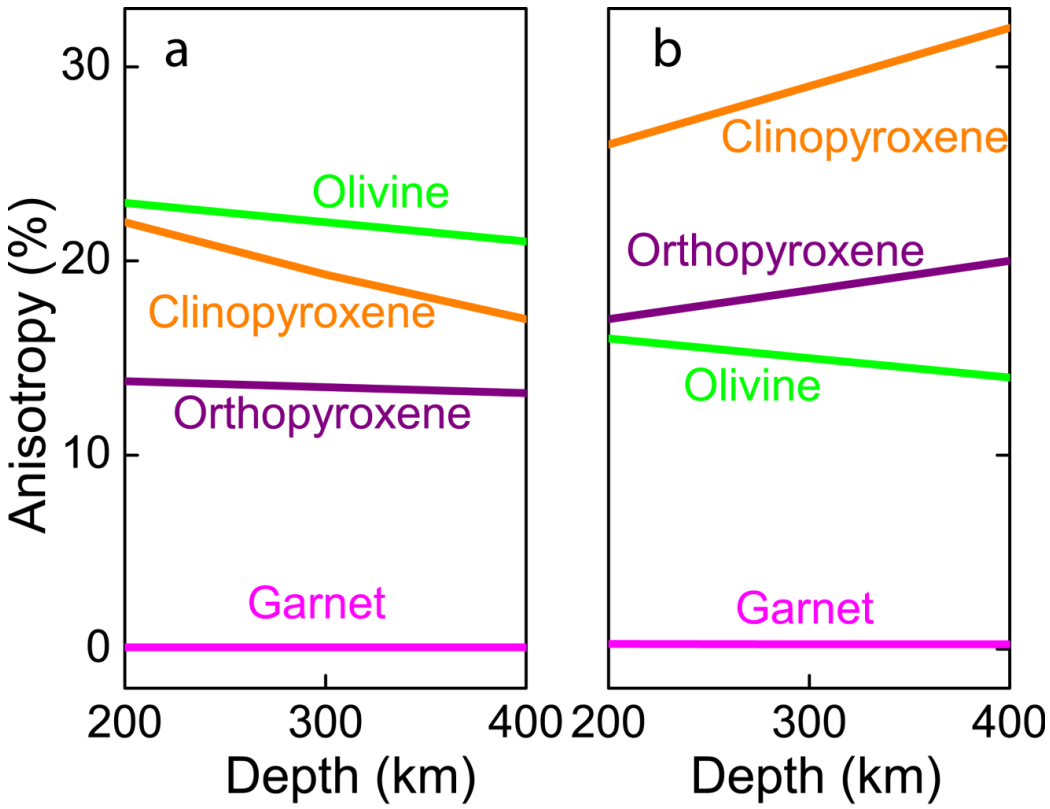

Fig. 7: Compressional-(V_P) (a) and shear-wave (V_S) (b) anisotropy of major minerals in the upper mantle. The anisotropy factor (A) is defined by 2*(V_{max} - V_{min}) / (V_{max}+V_{min})*100% for both V_P and V_S (Mainprice 2000). Magenta lines: garnet, this study; green lines: olivine (Zha et al. 1998; Liu and Li 2006); orange lines: clinopyroxene (Cpx) (Frisillo and Barsch 1972; Levien et al. 1979; Matsui and Busing 1984; Collins and Brown 1998); purple lines: orthopyroxene (Opx) (Frisillo and Barsch 1972; Duffy and Anderson 1989; Chai et al. 1997)

condition of the upper mantle. The third-order Eulerian finite-strain equation (equation 2 and 3) (Birch 1978) and the third-order Birch-Murnaghan EoS (equation 7) (Birch 1947) were used to calculate the K_S, G, V_P and V_S of the Fe-bearing pyrope at high P-T. Our modeling here is limited to the region between 200 to 400 km depth because of the relatively large regional seismic variations observed above 200 km depth (e.g. Grand

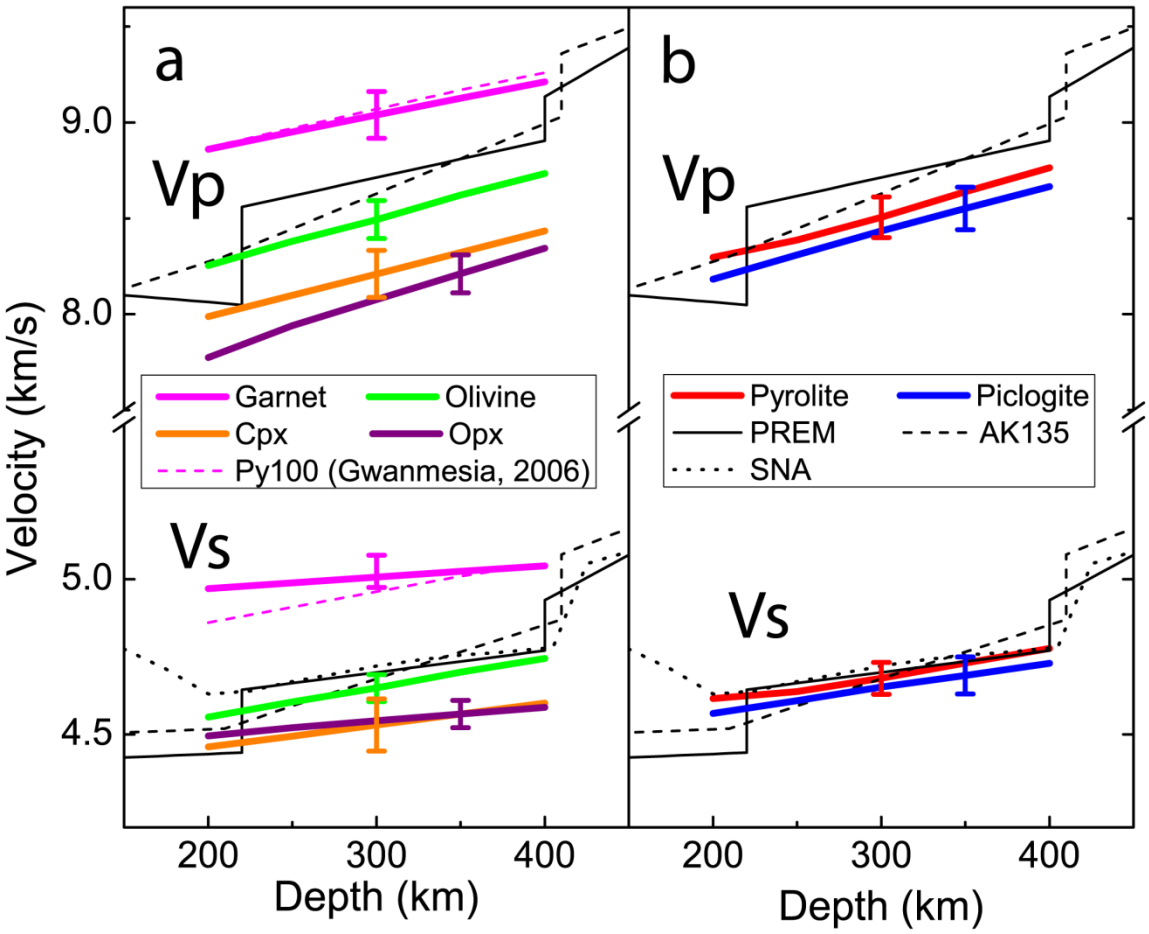

Fig. 8: Modeled velocities in the upper mantle. (a) Sound velocities of major minerals in the upper mantle compared with representative seismological models. Magenta solid lines: Fe-bearing pyrope (garnet), $(Mg_{2.4}Fe_{0.6})Al_2Si_3O_{12}$, in this study; magenta dash lines: garnet using elastic parameters of pure pyrope (Gwanmesia et al. 2006); green lines: olivine, $(Mg_{1.8}Fe_{0.2})SiO_4$ (Zha et al. 1998; Liu and Li 2006); orange lines: clinopyroxene (Cpx), $Ca(Mg_{0.9}Fe_{0.1})Si_2O_6$ (Sumino and Anderson 1984; Duffy and Anderson 1989; Zhang et al. 1997); purple lines: orthopyroxene (Opx), $Mg_{0.9}Fe_{0.1}SiO_3$ (Duffy and Anderson 1989; Angel and Hugh-Jones 1994; Chai et al. 1997b). (b) velocity model in pyrope (red) and piclogite (blue) composition. Seismic models in (a) and (b) inclide PREM in black solid lines (Dziewonski and Anderson 1981), AK135 in long dash lines (Kennett 1991) and SNA in dotted lines (Grand and Helmberger, 1984).

and Helmberger 1984). Compared with the modeled velocities of pure pyrope (Gwanmesia 2006) at the P-T conditions of 200 km depth, our results show that the Fe effect on elasticity of pyrope leads to a ~3% decrease in the V_S but negligible change in the V_P. In addition, the *Vp* and *Vs* profiles of olivine and pyroxene are also modeled using existing literature results on elasticity and thermodynamic parameters (Sumino and Anderson 1984; Duffy and Anderson 1989; Angel and Hugh-Jones 1994; Chai et al. 1997b; Zhang et al. 1997; Zha et al. 1998; Liu and Li 2006). The amount of iron in minerals is taken to be 10 mol% except for Mg-rich garnets (20 mol) following the estimation in Duffy and Anderson (1989).

Comparison between the modeled *Vp* and *Vs* profiles and representative global and regional seismic profiles in the region (Dziewonski and Anderson 1981; Grand and Helmberger 1984; Kennett 1991) shows that the *Vp* and *Vs* profiles of garnet are respectively ~4% and ~7% faster than the PREM and AK135 models (Dziewonski and Anderson 1981) (Fig. 8a). On the other hand, the *Vs* profile of olivine is very close to the seismic model but its *Vp* profile is slightly lower. Compared with garnet and olivine, the *Vp* and *Vs* profiles of pyroxene are ~5-7% and ~3-4 % slower than the seismic models, respectively.

We have further evaluated the effects of the volume fractions of these minerals in the pyrolite and piclogite compositional models of the upper mantle (Ringwood 1975; Anderson and Bass 1984; Ita and Stixrude, 1992) (Fig. 8b). The pyrolite and piclogite models represent two global mineral compositions of the upper mantle that are commonly used for comparison between mineral physics results and global seismic profiles (e. g.

Bass and Anderson 1984; Duffy and Anderson 1989; Cammarano et al. 2003; Li and Libermann 2007). The mineral assemblage in the pyrolite model includes ~63% olivine, ~15% garnet, ~16% clinopyroxene (Cpx), and ~6% orthopyroxene (Opx) (Ita and Stixrude 1992), while the piclogite model includes ~43% olivine, ~15% garnet, ~36% clinopyroxene, and ~6% orthopyroxene (Ita and Stixrude 1992). Our modeled *Vp* and *Vs* profiles for both pyrolite and piclogite models are very similar to each other within propagated experimental uncertainties, because the main difference in mineral assemblage in the piclogite model is that ~20% olivine in pyrolite model has been replaced by ~2-3% slower clinopyroxene. The pyrolite model appears to have slightly greater *Vp* and *Vs* velocities than the piclogite model because it contains more olivine and less clinopyroxene (Fig. 8b). Although the modeled *Vs* profiles of both pyrolite and piclogite models match well with the seismic profiles, their *Vp* profiles are approximately 2% lower than the PREM model, together with a small mismatch in the velocity gradient for both PREM and AK-135 models. The uncertainties we estimated in our results are only from the elasticity measurements themselves. In fact, the other uncertainties may also contribute to the misfit: the iron partitioning in different minerals may vary with depth; the anelastic effect in the upper mantle may need to be taken into the consideration (Karato 1995); the geotherm from different studies also have variations (e.g. Brown and Shankland 1981; Stacey 1992), etc. On the other hand, at the same depth, the seismic velocities from 1-D global seismic velocity models are also different (e.g. Dziewonski and Anderson 1981; Kennett 1991). Even though a lot of effort has been made on this type of test and comparison (e.g. Bass and Anderson 1984; Duffy and Anderson 1989;

Cammarano et al. 2003; Li and Libermann 2007), if we take these uncertainties into account, a lot more work is still needed to be done before we are able to constrain the mineralogical structure of our Earth.

Chapter 5: Conclusion

In summary, we report our new single-crystal elasticity results of natural Fe-bearing pyrope, $Mg_{2.04}Fe_{0.74}Ca_{0.16}Mn_{0.05}Al_2Si_3O_{12}$, using *in situ* Brillouin spectroscopy and X-ray diffraction at simultaneous high P-T conditions up to 20 GPa and 750 K. Our results indicate that addition of 25% Fe in pyrope increases the pressure derivative of the bulk modulus by 7%, while it doesn't the other elastic parameters significantly. Applying our updated single-crystal elasticity results on Fe-bearing pyrope, we have confirmed the former estimation that pyrope remains almost elastically isotropic at relevant P-T conditions of the upper mantle. Thus it may not have a significant contribution to seismic *Vp* and *Vs* anisotropy in the upper mantle. We also have constructed new velocity profiles for pyrolite and piclogite models, using our results and the elasticity of the other major minerals in the upper mantle. These velocity models show *Vs* profiles consistent with seismic observations, while *Vp* profiles are slightly lower than in seismic models.

Appendix A: Brillouin Scattering Method

When the incident monochromatic beam propagates through a medium, the photons interact with the medium to create phonons. The interaction thus can change the frequency of the scattered beam by an amount that depends on the phase velocity of the acoustic wave. This is the definition of Brillouin scattering. The interaction could be considered as one type of inelastic scattering, and the conservation of momentum and energy yield:

$$\overrightarrow{k_s} = \overrightarrow{k_\iota} \pm \vec{q}$$

$$\omega_s = \omega_0 \pm \omega_q$$

where $\vec{q}$ is wave vector of phonons, $\overrightarrow{k_\iota}$ and ω_0 are the wave vector and frequency of the incident beam, while $\overrightarrow{k_s}$ and ω_s are the wave vector and frequency of the scattered beam. The phonon wave vector $\vec{q}$ and incident wave vector $\overrightarrow{k_\iota}$ have the relationship:

$$|\vec{q}| = \left|\overrightarrow{k_s} - \overrightarrow{k_\iota}\right|$$

Considering the fact that the frequency of acoustic velocities is much smaller than the light frequency, thus:

$$|\vec{q}| = 2n\left|\overrightarrow{k_\iota}\right| \sin\frac{\theta}{2}$$

$$\omega_q = 2nv\left|\overrightarrow{k_\iota}\right| \sin\frac{\theta}{2}$$

where n is the refractive index and v is the acoustic velocity. Thus, we are able to measure the sound velocity directly by measuring the frequency shift of photon before and after the interaction.

Appendix B: Representative Pyrolite and Piclogite Composition

	Pyrolite* (wt%)	Piclogite** (wt%)
SiO_2	45.2	47.79
MgO	37.5	32.35
FeO	8.1	7.21
Al_2O_3	3.9	3.44
CaO	3.8	9.22
TiO_2	0.3	--
Cr_2O_3	0.5	--
Na_2O	0.3	--
NiO	0.3	--

*Pyrolite model (Ringwood 1975)
**Piclogite model (Anderson and Bass 1984; Duffy and Anderson 1989)

References

Anderson, D.L. and Bass, J.D. (1984) Mineralogy and composition of the upper mantle. Geophysical Research Letters, 11, 637-640.

Ando, M., Ishikawa, Y., and Wada, H. (1979) S-wave anisotropy in the upper mantle under a volcanic area in Japan. Nature, 286, 43-46.

Angel, R.J. and Hugh-Jones, D.A. (1994) Equations of state and thermodynamic properties of enstatite pyroxenes. Journal of Geophysical Research, 99, 19777-19783.

Bass, J.D. and Anderson, D.L. (1984) Composition of the upper mantle: geophysical tests of two petrological models. Geophysical Research Letters, 11, 237-240.

Birch, F. (1947) Finite elastic strain of cubic crystals. Physical Review, 71, 809-824.

Birch, F. (1978) Finite strain isotherm and velocities for single-crystal and polycrystalline NaCl at high pressures and 300 K. Journal of Geophysical Research, 83, 1257-1268.

Bonczar, L.J., and Graham, E.K. (1977) The pressure and temperature dependence of the elastic constants of pyrope garnet. Journal of Geophysical Research, 82, 2529-2534.

Brown, J.M. and Shankland, T.J. (1981) Thermodynamic parameters in the Earth as determined from seismic profiles. Geophysical Journal of the Royal Astronomical Society, 66, 579-596.

Cammarano, F., Goes, S., Vacher, P., and Giardini, D. (2003) Inferring upper-mantle temperatures from seismic velocities. Physics of the Earth and Planetary Interiors, 138,192-222.

Chai, M., Brown, J.M., and Slutsky, L.J. (1997a) The elastic constants of a pyrope-grossular-almandine garnet to 20 GPa. Geophysical Research Letters, 24, 523-526.

Chai, M., Brown, J.M., and Slutsky, L.J. (1997b) The elastic constants of an aluminous orthopyroxene to 12.5 GPa. Journal of Geophysical Research, 102, 14779-14785.

Chen, G., Miletich, R., Mueller, K., and Spetzler, H.A. (1997) Shear and compressional mode measurements with GHz ultrasonic interferometry and velocity-composition systematic for the pyrope-almandine solid solution series. Physics of the Earth and Planetary Interiors, 99, 273-287.

Chen, G., Cooke Jr., J.A., Gwanmesia, G.D., and Liebermann, R.C. (1999) Elastic wave velocities of Mg3Al2Si3O12-pyrope garnet to 10 GPa. American Mineralogist, 84, 384-388.

Collins, M.D., and Brown, J.M. (1998) Elasticity of an upper mantle clinopyroxene. Physics and Chemistry of Minerals, 26, 7-13.

Conrad, P.G., Zha, C.S., Mao, H.K., and Hemley, R.J. (1999) The high-pressure, single-crystal elasticity of pyrope, grossular, and andradite. American Mineralogist, 84, 374-383.

Dai, L. and Karato S. (2009) Electrical conductivity of pyrope-rich garnet at high temperature and high pressure. Physics of the Earth and Planetary Interiors, 176, 83-88.

Duffy, T.S. and Anderson, D.L. (1989) Seismic velocity in mantle minerals and mineralogy of the upper mantle. Journal of Geophysical Research, 94, 1895-1912.

Dziewonski, A.M. and Anderson, D.L. (1981) Preliminary reference Earth model. Physics of the Earth and Planetary Interiors, 25, 297-356.

Every, A.G. (1980) General closed-form expressions for acoustic waves in elastically anisotropic solids. Physics Review B, 22, 1746-1760.

Fei, Y. (1995) Mineral physics and crystallography. In T. Ahrens, Eds., a handbook of physical constants, AGU reference shelf 2, p. 29-44. American Geophysical Union, Washington, D.C.

Fei, Y. and Bertka, C.M. (1999) Phase transitions in the Earth's mantle and mantle mineralogy. In Y. Fei, C.M. Bertka and B.O. Mysen, Eds., Mantle Petrology: Field Observations and High Pressure Experimentation, vol. 6. p. 189-207. Spec. Publ. Geochem. Soc., Houston, TX.

Fei, Y., Ricolleau, A., Frank, M., Mibe, K., Shen, G., and Prakapenka, V. (2007) Toward an internally consistent pressure scale. Proceedings of the National Academy of Sciences, 104, 9182-9186.Giesting, P.A. and Hofmeister, A.M. (2002) Thermal conductivity of disordered garnets from infrared spectroscopy. Physical Review B, 65, 144305.

Frisillo, A.L., and Barsch, G.R. (1972) Measurement of single-crystal elastic constants of bronzite as a function of pressure and temperature. Journal of Geophysical Research, 77, 6360-6384.

Gillet, P., Fiquet G., Malezieux, J.M., and Geiger, C.A. (1992) High-pressure and high temperature Raman spectroscopy of end-member garnets: pyrope, grossular and andradite. European Journal of Mineralogy, 4, 651-664.

Grand, S.P. and Helmberger, D.V. (1984) Upper mantle shear structure of North America. Geophysical Journal Royal Astronomical Society, 76, 399-438.

Gwanmesia, G.D., Zhang, J., Darling, K., Kung, J., Li, B., Wang, L., Neuville, D., and Liebermann, R.C. (2006) Elasticity of polycrystalline pyrope to 9 GPa and 1000 ^{0}C. Physics of the Earth and Planetary Interiors, 155, 179-190.

Gwanmesia, G.D., Jackson, I., and Liebermann, R.C. (2007) In search of the mixed derivative ∂2M/∂P∂T (M=G, K): joint analysis of ultrasonic data for polycrystalline pyrope from gas- and solid-medium apparatus. Physics and Chemistry of Minerals, 34, 85-93.

Hess, H.H. (1964) Seismic anisotropy of the uppermost mantle under oceans. Nature, 203, 629-631.

Hill, R. (1952) The elastic behavior of a crystalline aggregate. Proceeding of the Physical Society of London, Section A, 65, 349-354.

Irifune, T. and Isshiki, M. (1998) Iron partitioning in a pyrolite mantle and the nature of the 410-km seismic discontinuity. Nature, 392, 702-705.

Irifune, T., Higo, Y., Inoue, T., Kono, Y., Ohfuji, H., and Funakoshi, K. (2008) Sound velocities of majorite garnet and the composition of the mantle transition region. Nature, 451, 814-817.

Ita, J. and Stixrude, L. (1992) Petrology, elasticity, and composition of the mantle transition zone. Journal of Geophysical Research, 97, 6849-6866.

Jacobsen, S.D., Reichmann, H.J. Spetzler, H.A., Mackwell, S.J., Smyth, J.R., Angel, R.J., and McCammon C.A. (2002) Structure and elasticity of single-crystal (Mg,Fe)O and a new method of generating shear waves for gigahertz ultrasonic interferometry. Journal of Geophysical Research, 107, B000490.

Jiang, F., Speziale, S., and Duffy, T.S. (2004) Single-crystal elasticity of grossular- and almandine-rich garnets to 11 GPa by Brillouin scattering. Journal of Geophysical Research, B10210.

Kanamori, H., Fujii, N., and Mizutani, H. (1968) Thermal diffusivity measurement of rock-forming minerals from 300 to 1100 K. Journal of Geophysical Research, 73, 595-605.

Karato, S. (1995) Effects of water on seismic wave velocities in the upper mantle. Proceeding of the Japan Academy, B, 71, 61-66.

Kawasaki, I. and Konno, F. (1984) Azimuthal anisotropy of surface-waves and the possible type of the seismic anisotropy due to preferred orientation of olivine in the uppermost mantle beneath the Pacific-ocean. Journal of Physics of the Earth, 32, 229-244.

Kennett, B.L.N. (1991) Seismic velocity gradients in the upper mantle. Geophysical Research Letters, 18, 1115-1118.

Kennett, B.L.N. Engdahl, E.R., and Buland R. (1995) Constraints on seismic velocities in the Earth from traveltimes. Geophysical Journal International, 122, 108-124.

Lee, C.-T. A. (2003) Compositional variation of density and seismic velocities in natural peridotites at STP conditions: Implications for seismic imaging of compositional

heterogeneities in the upper mantle. Journal of Geophysical Research, 108, 2441-2461.

Leitner, B.J., Weidner, D.J., and Liebermann, R.C. (1980) Elasticity of single crystal pyrope and implications for garnet solid solution series. Physics of the Earth and Planetary Interiors, 22, 111-121.

Levien, L., Weidner, D.J., and Prewitt, C.T. (1979) Elasticity of diopside. Physics and Chemistry of Minerals, 4, 105-113.

Li, B. and Libermann, R.C. (2007) Indoor seismology by probing the Earth's interior by using sound velocity measurements at high pressures and temperature. Proceedings of the National Academy of Sciences, 104, 9145-9150.

Liu, W. and Li, B. (2006) Thermal equation of state of (Mg0.9Fe0.1)2SiO4 olivine. Physics of the Earth and Planetary Interiors, 2006, 188-195.

Mainprice, D. and Nicolas, A. (1989) Development of shape and lattice preferred orientations: application to the seismic anisotropy of the lower crust. Journal of Structural Geology, 11, 175-189.

Mainprice, D., Barruol, G., and Ben Ismail, W. (2000) The anisotropy of the Earth's mantle: From single crystal to polycrystal. In S. Karato, A.M. Forte, R.C. Liebermann, G. Masters and L. Stixrude, Eds., AGU Geophysical Monograph 117. American Geophysical Union, Washington, D.C.

Mao, H.K., Xu, J., and Bell, P.M. (1986) Calibration of the ruby pressure gauge to 800 kbar under quasi-hydrostatic conditions. Journal of Geophysical Research, 91, 4673-4676.

Marquardt, H., Ganschow, S., and Schilling, F.R. (2009) Thermal diffusivity of natural and synthetic garnet solid solution series. Physics and Chemistry of Minerals, 36, 107-118.

Matsui, M., and Busing, W.R. (1984) Calculation of the elastic constants and high-pressure properties of diopside, $CaMgSi_2O_6$. American Mineralogist, 69, 1090-1095.

Montagner, J.P. and Tanimoto, T. (1990) Global anisotropy in the upper mantle inferred from the regionalization of phase velocities. Journal of Geophysical Research, 95, 4797-4819.

Montagner, J.P. and Kennett, B.L.N. (1995) How to reconcile body-wave and normal-mode reference Earth models? Geophysical Journal International, 1995, 229-248.

O'Neill, B., Bass, J.D., Rossman, G.R., Geiger, C.A., and Langer, K. (1991) Elastic properties of pyrope. Physics and Chemistry of Minerals, 17, 617-621.

Poli, S. (1993) The amphibolite-eclogite transformation: an experimental study on basalt. American Journal of Science, 293, 1061-1107.

Raitt, R.W., Shor, G.G., Francis, T.J.G., and Morris, G.B. (1969) Anisotropy of the Pacific upper mantle. Journal of Geophysical Research, 74, 3095-3190.

Rickwood, P.C., Mathias, M., and Siebert, J.C. (1968) A study of garnets from eclogite and peridotite xenoliths found in kimberlite. Contributions to Mineralogy and Petrology, 19, 271-301.

Ringwood, A.E. (1967) Pyroxene-garnet transformation in Earth's mantle. Earth and Planetary Science Letters, 2, 255-263.

Ringwood, A.E. (1975) Composition and petrology of the Earth's Mantle, p. 618. McGraw-Hill, New York.

Ringwood, A.E. (1991) Phase transformations and their bearing on the constitution and dynamics of the mantle. Geochimica et Cosmochimica Acta, 55, 2083-2110.

Romano, C., Poe, B.T., Kreidie, N., and McCammon, C. (2006) Electrical conductivities of pyrope-almandine garnets up to 19 GPa and 1700 ^{0}C. American Mineralogist, 91, 1371-1377.

Silver, P.G. and Chan, W.W. (1991) Shear wave splitting and subcontinental mantle deformation. Journal of Geophysical Research, 96, 16429-16454.

Sinogeikin, S.V. and Bass, J.D. (2000) Single-crystal elasticity of pyrope and MgO to 20 GPa by Brillouin scattering in the diamond cell. Physics of the Earth and Planetary Interiors, 120, 43-62.

Sinogeikin, S.V. and Bass, J.D. (2002) Elasticity of pyrope and majorite-pyrope solid solutions to high temperatures. Earth and Planetary Science Letters, 203, 549-555.

Soga, N. (1967) Elastic constants of garnet under pressure and temperature. Journal of Geophysical Research, 72, 4227-4234.

Stacey, F.D. (1992) Physics of the Earth. Brookfield Press, Brisbane, Australia.

Sumino, Y. and Nishizawa, O. (1978) Temperature variation of elastic constants of pyrope almandine garnets. Journal of Physics of the Earth, 26, 239-252.

Suzuki, I. and Anderson, O.L. (1983) Elasticity and thermal expansion of a natural garnet up to 1000K. Journal of Physics of the Earth, 31, 125-138.

Verma, R.K. (1960) Elasticity of some high-density crystals. Journal of Geophysical Research, 65, 757-766.

Wang, Z. and Ji, S. (2001) Elasticity of six polycrystalline silicate garnets at pressure up to 3.0 GPa. American Mineralogist, 86, 1209-1218.

Webb, S.L. (1989) The elasticity of the upper mantle orthosilicats olivine and garnet to 3 GPa. Physics and Chemistry of Minerals, 16, 684-692.

Zha, C.S., Duffy, T.S., Downs, R.T., Mao, H.K., and Hemley, R.J. (1998) Brillouin scattering and X-ray diffraction of San Carlos olivine: direct pressure determination to 32 GPa. Earth and Planetary Science Letters, 159, 25-33.

Zhang, L., Ahsbahs, H., Hafner, S.S., and Kutoglu, A. (1997) Single-crytstal compression and crystal structure of clinopyroxene up to 10 GPa. American Mineralogist, 82, 245-258.